An Improved Nonlinear Flux Observer Based Sensorless FOC IM Drive With Adaptive Predictive Current Control

Ambrish Devanshu, Madhusudan Singh, *Senior Member, IEEE*, and Narendra Kumar, *Senior Member, IEEE*

***Abstract*—This paper presents a novel adaptive predictive current controller (PCC) with improved flux estimator for a sensorless direct field oriented control (DFOC) induction motor (IM) drive. Classical PCC performance depends on the stator resistance of the motor which varies with temperature. In the proposed method, a discrete stator resistance estimator is developed to increase the robustness of the system toward stator resistance variations. An improved nonlinear discrete stator flux estimator is also developed to replace the pure integrator which reduces the initial value and dc offset problems. Sensorless operation of IM drive has advantages of reduced overall cost and increased reliability of motor operation. Dynamic and steady-state performances of the IM under different operating conditions are analyzed in MATLAB/Simulink as well as experimentally using dSPACE1104 controller and have been compared with conventional PCC. The simulation results of the classical and proposed methods are also validated experimentally. Smooth starting, reduced oscillations in speed and flux at low speed operation, fast speed and torque dynamics, robust operation of drive against load and variation in stator resistance, fast and smooth speed reversal are the main advantages of the proposed method over classical PCC-based DFOC IM drive.**

***Index Terms*—Discrete, field oriented control, induction motor (IM), integration, predictive current control (PCC), transform.**

I. Introduction

THE induction motor (IM) is widely used in industry due to its low cost, less maintenance, and rugged construction. With the advancement in the different control techniques of the IM, several current-regulation methods have been developed for control of voltage source inverter (VSI) fed IM drives. These advance control methods of the IM can provide high performance, high accuracy, fast dynamic response, and excellent tracking ability of the drive. The different current-regulation techniques such as hysteresis control, linear pulsewidth modulator (PWM), predictive control, sliding mode control, delta and sigma delta modulation, neural networks, fuzzy logic, and neuro-fuzzy controls can be used to minimize the current ripple and improve the performance of the IM drives [1]. Recent evolution in the digital electronics and availability of faster and more powerful processors with the high computational speed, predictive current control (PCC) has emerged as a powerful current control method which provides switching signals to solid state switches in VSI based on optimized algorithm and cost function [1], [8]. Generalized predictive control (GPC) technique has been applied to current source inverter for the regulation of the current to the resistive inductive circuit model of the IM [2]. The GPC is developed in synchronously rotating reference frame and play useful role in the control of stator current of the IM [3]. Based on the electromotive force concept, current controller has been developed which requires one period prediction and delay introduced by the measurement. It is reported that this control technique is more affected by the variations in load inductances than the rotor and stator resistances [4], [5]. A PCC based on space vector modulation is proposed using discrete motor modeling [6]. The performance of the PCC method proposed in [7] is being compared with PWM and hysteresis current controller. In this method, for all the value of voltage vectors, predicted value of load current is generated by the inverter. Long range model based PCC is designed for an input–output linearized IM [9]. However, modeling of the inverter is not taken into account in the conventional FOC. Whereas, state of the inverter is defined as discrete control variable when PCC strategy is used. Flux and time constant of the rotor is estimated using reduced order extended high gain observer [10]. An improved version of PCC is proposed [11] which considers a control technique of neutral point potential and optimized description of inverter switching transitions. This approach enables fast motor current control while maintaining a low switching and excluding excitation of the filter resonance. The FOC of five-phase IM is discussed for the verification of the model predictive control to achieve ripple free stator current and fast current response [12]. It has been observed that predictive control method offers faster torque and current response than PI controllers [13] with SVPWM techniques for multiphase drives. However, PCC technique is implemented for speed sensorless FOC IM drive system along with SVPWM to ensure fixed switching frequency [14].

The bandwidth of the traditional current controller with PI regulator is limited by the switching frequency and this limitation is removed by the PCC in sensorless FOC system [15].

Manuscript received November 7, 2018; revised January 14, 2019; accepted April 14, 2019. Date of publication April 18, 2019; date of current version October 18, 2019. Recommended for publication by Associate Editor R. Kennel. *(Corresponding author: Ambrish Devanshu.)*

The authors are with the Electrical Engineering Department, Delhi Technological University, Delhi 110042, India (e-mail: ambrish.devanshu@gmail.com; madhusudan@dce.ac.in; ndeshwalus@gmail.com).

Color versions of one or more of the figures in this paper are available online at http://ieeexplore.ieee.org.

Digital Object Identifier 10.1109/TPEL.2019.2912265

For managing post fault operation of multiphase drives, PCC is being proposed [16]. An improved current control in IM, robust PCC is implemented based on polytopic uncertainties and linear matrix inequalities. Offline multiparametric semidefinite programming and quadratic search tree is applied for the current control resulting into significantly suppressed overshooting [17]. The dynamic performance of the current loop is also improved using robust PCC combined with a speed adaptive full order observer [18].

The classical PCC has drawbacks of large torque and flux ripple, large THDs in voltages and currents and dependency on the motor parameter such as stator resistance. Slip speed of the IM drive also depends on the rotor time constant of the motor. The rotor and stator resistance are important parameters of IM whose variations may lead to improper performance of the PCC and improper estimation of speed over the wide operating range in sensorless drives [25].

An adaptive PCC is implemented in this paper and stator resistance is estimated to overcome the uncertainty due to the stator resistance variations. The rotor time constant is also estimated using Popov's stability criteria as slip speed depends on this parameter of the motor. For the correct estimation of the parameters and high performance of the drive, accurate information of the fluxes is also needed. Additionally, in the stator voltage model of the flux estimation, an integrator is being used in the majority of the work reported in the literature [19]–[22]. However, existing dc drift in the system and initial value of the pure integrator will cause integrator to saturate resulting into distorted estimated flux. Thus, an improved nonlinear discrete stator flux estimator is also proposed to replace the pure integrator to reduce the dc offset and initial value problem. The sensorless direct field oriented control (DFOC) IM drive with nonlinear flux observer and adaptive PCC is analyzed in MATLAB/Simulink as shown in Fig. 1(a). A complete experimental setup of DFOC IM drive with estimators is implemented in the laboratory using dSPACE 1104 controller. The simulation and experimental results are discussed for sensorless speed control of IM to validate the effectiveness of the proposed estimation and control algorithms. A comparison of the IM drive performance with conventional PCC and proposed PCC method shows that the proposed method can effectively improve the overall performance of the drive.

In this paper, the major contributions on DFOC IM drive by the authors are as follows.

1) Performance of the system for DFOC IM drive is analyzed. An adaptive PCC is developed for more robust performance of the DFOC IM motor drive.
2) Discrete stator resistance estimator is established for the controller to adapt for changes in stator resistance of the IM. The rotor time constant of the motor is also calculated using Popov's stability criteria.
3) A discrete nonlinear stator and rotor flux observer is developed to mitigate the effect of the existing dc offset problem in the system due to inverter nonlinearity, current measurement, biasing in sensors, operational amplifier, A/D converter, variations in stator resistance, and unknown integral initial conditions at the starting of the drive.

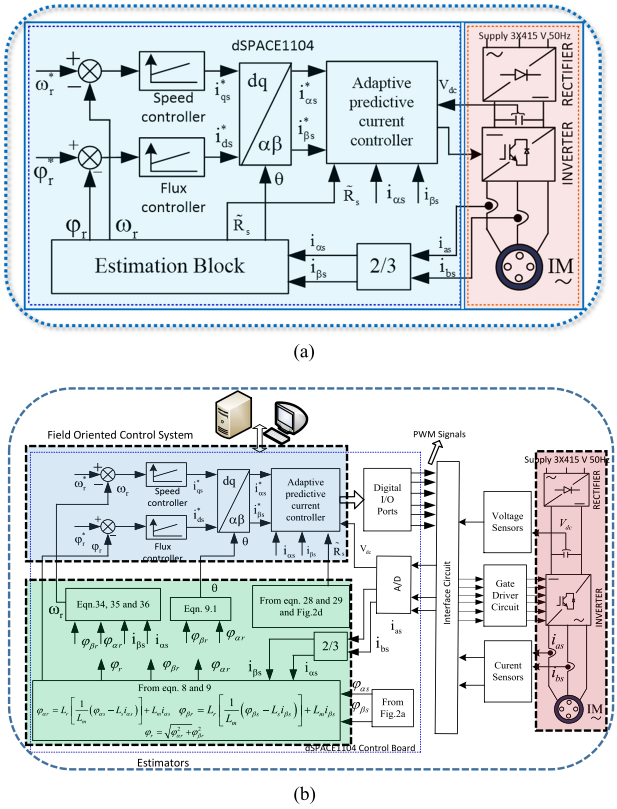

Fig. 1. (a) Block diagram of proposed DFOC IM drive. (b) Simulation and experimental schematic diagram of proposed method with estimators.

4) Mechanical sensorless technique with proposed stationary discrete nonlinear flux observer is developed to minimize the cost of the system.

II. Mathematical Modeling of IM

Dynamic modeling of the IM in stationary reference frame is described by the following state equations:

$$\begin{aligned} \dot{x} &= Ax + Bu \\ y &= Cx \end{aligned} \tag{1}$$

where

$$A = \begin{bmatrix} -\left(\frac{L_m^2}{\sigma L_s L_r \tau_r} + \frac{R_s}{\sigma L_s}\right) & 0 & \frac{L_m}{\sigma L_s L_r \tau_r} & \frac{L_m \omega_r}{\sigma L_s L_r} \\ 0 & -\left(\frac{L_m^2}{\sigma L_s L_r \tau_r} + \frac{R_s}{\sigma L_s}\right) & \frac{L_m \omega_r}{\sigma L_s L_r} & \frac{L_m}{\sigma L_s L_r \tau_r} \\ \frac{L_m}{\tau_r} & 0 & -\frac{1}{\tau_r} & -\omega_r \\ 0 & \frac{L_m}{\tau_r} & -\omega_r & \frac{1}{\tau_r} \end{bmatrix}$$

$$B = \begin{bmatrix} \frac{1}{\sigma L_s} & 0 & 0\ 0 \\ 0 & \frac{1}{\sigma L_s} & 0\ 0 \end{bmatrix}$$

$$C = \begin{bmatrix} 1\ 0\ 0\ 0 \\ 0\ 1\ 0\ 0 \end{bmatrix}$$

$$x = [i_{\alpha s}\ i_{\beta s}\ \varphi_{\alpha r}\ \varphi_{\beta r}]^T$$

$$u = [u_{\alpha s}\ u_{\beta s}\ 0\ 0]^T \tag{1}$$

$$\omega_r = 1/J \int (T_e - T_L)dt \tag{2}$$

$$Te = \frac{3PL_m}{4L_r}\left(i_{\beta s}\varphi_{\alpha r} - i_{\alpha s}\varphi_{\beta r}\right) \tag{3}$$

where R_s is stator resistance per phase, L_m is magnetizing inductance per phase, R_r is rotor resistance per phase, L_r is rotor inductance per phase, $L_s =$ stator inductance per phase, L_m is magnetizing inductance per phase, P is number of poles, ω_r is rotor electrical angular speed, J is the moment of inertia of rotor, T_e is the electromagnetic torque, T_l is the external load torque, $u_{\beta s}$ ($u_{\alpha s}$) is β-axis (α-axis) stator voltage, $i_{\beta s}$($i_{\alpha s}$) is β-axis (α-axis) stator current, $\varphi_{\beta r}(\varphi_{\alpha r})$ is β-axis (α-axis) rotor flux, and $\sigma = 1 - (L_m^2/L_r L_s)$.

III. Direct Field Oriented Control of IM Drive

Field oriented control of IM is implemented by independent control of field flux component and the torque component of the stator current. The torque component of the stator current is in the quadrature of the rotor flux and flux component of the current is oriented in phase of it. Following equations are used for the implementation of DFOC IM drive:

Motor stator terminal voltages and currents are sensed and fluxes are computed in stationary reference frame as follows:

$$\begin{bmatrix} u_{\alpha s} \\ u_{\beta s} \end{bmatrix} = \begin{bmatrix} \frac{2}{3} & -\frac{1}{3} & \frac{1}{3} \\ 0 & \frac{2}{\sqrt{3}} & -\frac{2}{\sqrt{3}} \end{bmatrix} \begin{bmatrix} u_{as} \\ u_{bs} \\ u_{cs} \end{bmatrix},$$

$$\begin{bmatrix} i_{\alpha s} \\ i_{\beta s} \end{bmatrix} = \begin{bmatrix} \frac{2}{3} & -\frac{1}{3} & \frac{1}{3} \\ 0 & \frac{2}{\sqrt{3}} & -\frac{2}{\sqrt{3}} \end{bmatrix} \begin{bmatrix} i_{as} \\ i_{bs} \\ i_{cs} \end{bmatrix} \tag{4}$$

where u_{as}, u_{bs}, and u_{cs} are stator three phase terminal voltage and i_{as}, i_{bs}, and i_{cs} are stator line currents.

Stator flux equations of IM are written as follows:

$$\varphi_{\alpha s} = \int (u_{\alpha s} - i_{\alpha s}R_s)\, dt,\ \varphi_{\beta s} = \int (u_{\beta s} - i_{\beta s}R_s)\, dt \tag{5}$$

$$\varphi_{\alpha s} = L_s i_{\alpha s} + L_m i_{\alpha r},\ \varphi_{\beta s} = L_s i_{\beta s} + L_m i_{\beta r}. \tag{6}$$

Resultant stator flux φ_s and phase angle θ_s between $\varphi_{\alpha s}$ and $\varphi_{\beta s}$ can be evaluated as follows:

$$\varphi_s = \sqrt{\varphi_{\alpha s}^2 + \varphi_{\beta s}^2},\ \theta_s = \tan^{-1}\left(\varphi_{\beta s}/\varphi_{\alpha s}\right). \tag{7}$$

Rotor currents are determined as follows:

$$i_{\alpha r} = \frac{1}{L_m}\left(\int (u_{\alpha s} - i_{\alpha s}R_s)\, dt - L_s i_{\alpha s}\right),$$

$$i_{\beta r} = \frac{1}{L_m}\left(\int (u_{\beta s} - i_{\beta s}R_s)\, dt - L_s i_{\beta s}\right). \tag{8}$$

Therefore, rotor flux is evaluated as follows:

$$\varphi_{\alpha r} = L_r i_{\alpha r} + L_m i_{\alpha s},$$

$$\varphi_{\beta r} = L_r i_{\beta r} + L_m i_{\beta s},\ \varphi_r = \sqrt{\varphi_{\alpha r}^2 + \varphi_{\beta r}^2} \tag{9}$$

$$\theta_r = \tan^{-1}\left(\varphi_{\beta r}/\varphi_{\alpha r}\right). \tag{9.1}$$

IV. Flux Estimation Using Modified Integration

The high performance motor drives such as field oriented control, direct torque control, and feedback linearization control of ac drives require an accurate estimation of flux. Estimation of flux is usually implemented using two existing methods namely voltage model and current model. The voltage model for stator flux estimation is being considered in this paper. Estimation of stator flux using voltage model requires pure integrator, which creates drift signal component caused by the inverter problems [20], [21]. To eliminate the drawbacks of a pure integrator in voltage model based stator flux estimation, a low-pass filter (LPF) with feedback compensation integration algorithm is implemented as shown in Fig. 2(a)–(b). The stator flux estimated using modified integration is described as follows:

$$\varphi_s = e_s \frac{1}{s+\omega_c} + \varphi_s^L \frac{\omega_c}{s+\omega_c},\ \varphi_s = \varphi_s^F + \varphi_s^C \tag{10}$$

where

$$\varphi_s^F = e_s \frac{1}{s+\omega_c} \text{ and } \varphi_s^C = \varphi_s \frac{\omega_c}{s+\omega_c}. \tag{11}$$

First part of the (10) is a LPF and second part is a compensating feedback signal which is used to counterbalance the error in the output. The term φ_s^L is the output of the saturation block used to stop the integration as soon as signals go above the reference stator flux amplitude. The value of φ_s^L is obtained using the stator angle which is calculated from flux components $\varphi_{\alpha s}$ and $\varphi_{\beta s}$. Therefore, the accuracy of the estimated flux is strongly dependent on the angle θ_s given in (7). Application of this method at lower frequency of operation for IM leads to improvement in the ripple in flux, torque, and speed.

Several discretization methods for second-order generalized integrator are implemented [19]. For the implementation of the discrete flux controller, modified integrator (11) can be expressed as follows:

$$e_s = \varphi_s^F(s+\omega_c),\ e_s = \varphi_s^F \times s + \varphi_s^F \times \omega_c. \tag{12}$$

In order to achieve the better performance, advanced numerical method such as trapezoidal method for discrete time integration is used for the flux estimation [22]. In trapezoidal method, integrator is defined as $1/s = \frac{T_s}{2}\frac{z+1}{z-1}$.

In this way, realization of (12) in discrete form can be written as

$$\varphi_s^F(k) = \frac{T_s + T_s z^{-1}}{(\omega_c T_s + 2) + (\omega_c T_s - 2)\, z^{-1}}. \tag{13}$$

Similarly, second term of the (10) is the compensating feedback signal in the discrete form can be written as

$$\varphi_s^C(k) = \frac{\omega_c T_s + \omega_c T_s z^{-1}}{(\omega_c T_s + 2) + (\omega_c T_s - 2)\, z^{-1}}. \tag{14}$$

Realization of (13) and (14) in MATLAB/Simulink is shown Fig. 2(a).

V. Adaptive Predictive Current Controller

The predictive control is an advanced and powerful control with ability to consider constraints and actuators limitations.

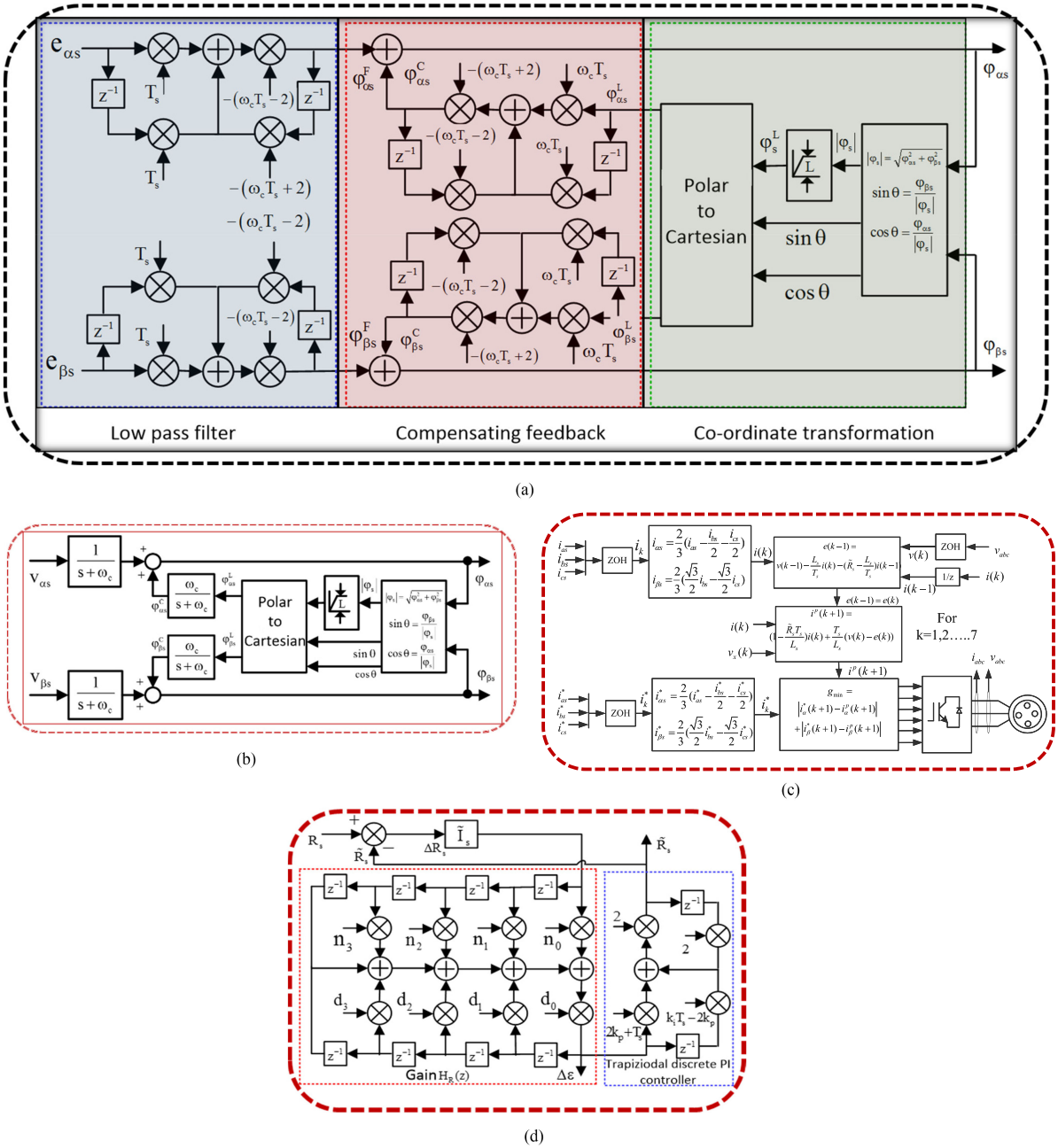

Fig. 2. (a) Discrete time realization of modified flux integration. (b) Modified flux integration in s-domain. (c) Block diagram of PCC. (d) Discrete time realization of stator resistance estimation.

The adaptive PCC has been used in the IM drive system specially to achieve good performance at a low speed operation and satisfactory robustness in drive operation. Fig. 2(c) shows the basic principle of the proposed adaptive PCC.

A. Objective Function

The IM is considered as a combination of resistance, inductance, and back-emf for VSI which is used to predict the nature of the stator currents for every switching state generated by VSI. An objective function is defined for the selection of the best switching state which is applied to control VSI and this objective function is calculated for the predicted values to be controlled. The error signal between predicted stator currents and reference stator currents minimized using the cost function defined with PCC [6], [7], [24]. The best switching state which gives the minimum value of cost function is selected and applied to the three-leg VSI without any use of modulation stage and linear regulators. The error between reference currents generated using indirect FOC and predicted currents are measured by cost function which is expressed in vector form as

$$\vec{g} = \vec{i}^{*}(k+1) - \vec{i}^{p}(k+1) \tag{15}$$

where $\vec{i}^{*}(k+1) = \vec{i}^{*}_{\alpha}(k+1) + j\vec{i}^{*}_{\beta}(k+1)$ and $\vec{i}^{p}(k+1) = \vec{i}^{p}_{\alpha}(k+1) + j\vec{i}^{p}_{\beta}(k+1)$.

Here, $\vec{i}^*(k+1)$ is the reference stator current vector produced using DFOC algorithm, $\vec{i}^*_\alpha(k+1)$ and $\vec{i}^*_\beta(k+1)$ are the real and fictitious constituent of this current vector, $\vec{i}^p(k+1)$ is the predicted stator current vector. Currents $\vec{i}^p_\alpha(k+1)$ and $\vec{i}^p_\beta(k+1)$ are the real and fictitious constituent of the current vector $\vec{i}^p(k+1)$ for a given voltage vector. Superscript "p" is used for the predicted variables. Now, the objective function in $\alpha\beta$ coordinate system can be defined for every voltage vector as

$$\vec{g} = |i^*_\alpha(k+1) - i^p_\alpha(k+1)| + |i^*_\beta(k+1) - i^p_\beta(k+1)|. \quad (16)$$

B. Modeling of Voltage Source Inverter

A the three-phase VSI is comprised of six insulated gate bipolar transistor (IGBT) switches (S_1 S_2 …S_6), which forms three-leg of VSI. Each leg of VSI is controlled in complementary mode. Different switching states of the VSI are governed by the gating signals S_a, S_b, and S_c as follows:

$$S_a = \begin{cases} 1 \text{ if } S_1 \text{ ON and } S_4 \text{ OFF} \\ 0 \text{ if } S_1 \text{ OFF and } S_4 \text{ ON} \end{cases}$$

$$S_b = \begin{cases} 1 \text{ if } S_2 \text{ ON and } S_5 \text{ OFF} \\ 0 \text{ if } S_2 \, OFF \text{ and } S_5 \text{ ON} \end{cases}$$

$$S_c = \begin{cases} 1 \text{ if } S_3 \text{ ON and } S_6 \text{ OFF} \\ 0 \text{ if } S_3 \text{ OFF and } S_6 \text{ ON.} \end{cases}$$

The value of output voltage generated by inverter with different switching signals can be defined as

$$v = V_{\rm dc} S \quad (17)$$

where $S = 2/3(S_a + aS_b + a^2 S_c)$ is the inverter switching state vector and $v = 2/3(v_{aN} + av_{bN} + a^2 v_{cN})$ is the output voltage vector generated by the inverter. $V_{\rm dc}$ is the dc link voltage, $a = e^{j2\Pi/3}$ is the unitary vector which gives 120° phase shift in different phases. For simplicity, diode forward voltage, dead time, and IGBT saturation voltage is not considered in this inverter model.

C. Discrete Time Model for Prediction

A discrete model considering IM as load on the inverter is developed here. From equivalent circuit of the IM, the continuous time model equation is written as

$$v = i\tilde{R}_s + L_s \frac{di}{dt} + e \quad (18)$$

where *v* and *i* are the voltage and current vector produced at the inverter terminal, which is also stator voltage and stator current for the IM, *e* is back-emf vector of IM. At the *k*th sampling instant, stator voltage, and current is predicted here using discrete time model of the stator current. Sampling time used for the entire discretization process is T_s. Using the forward Euler approximation, stator current derivative *di/dt* can be written as

$$\frac{di}{dt} \approx \frac{i(k+1) - i(k)}{T_s}. \quad (19)$$

For every voltage vector $v_x(k)$ which is produced by the inverter, future stator current can be predicted by substituting the value of $\frac{di}{dt}$ in (18) from (19) as

$$i^p(k+1) = \left(1 - \frac{\tilde{R}_s T_s}{L_s}\right) i(k) + \frac{T_s}{L_s}(v(k) - e(k)). \quad (20)$$

Using (20) back-emf can be calculated as

$$e(k-1) = v(k-1) - \frac{L_s}{T_s} i(k) - \left(\tilde{R}_s - \frac{L_s}{T_s}\right) i(k-1). \quad (21)$$

Using an extrapolation of past back-emf $e(k-1)$, the present value $e(k)$ of the back-emf can be estimated. Further, the value of sampling frequency is much larger than the frequency of the back-emf and it is assumed that back-emf will not change significantly in one sampling period. Therefore, it is assumed that $e(k) = e(k-1)$.

D. Adaptive Predictive Current Controller Algorithm

A block diagram of PCC is shown in Fig. 2(c). It shows the implementation of control algorithm for PCC used for DFOC IM drive system. Reference currents are being generated from DFOC IM drive system where one PI controller is used for the regulation of the speed and rotor flux. The three phase stator current i_{abc} are measured from the stator terminals of IM and the reference stator current i^*_{abc} are calculated from DFOC method. The back-emf is calculated with the help of discrete stator current and voltage vector at the motor stator terminals. Predicted current $i_p(k+1)$ is determined for back-emf $e(k)$ and each voltage vector $v(k)$. The error between predicted stator current and reference current generated using control algorithm is minimized using minimum function block of the MATLAB/Simulink for each voltage vector for each sampling interval. The best switching state which gives the minimum value of cost function are selected and applied to control the three-leg VSI.

VI. Parameter Adaptation

A. Stator Resistance Adaptation

The state-space representation of the machine in stationary reference frame with stator current and rotor flux as state variables, are given in (1). On linearization of (1), the linearized equations can be written as

$$\Delta \dot{x} = A\Delta x + B\Delta u + \Delta A x_0 \quad (22)$$

$$\Delta y = C\Delta x \quad (23)$$

where

$$x_0 = \begin{bmatrix} i_{\alpha s0} & i_{\beta s0} & \varphi_{\alpha r0} & \varphi_{\beta r0} \end{bmatrix}^T$$

$$\Delta u = \begin{bmatrix} \Delta u_{\alpha s} & \Delta u_{\beta s} & 0 & 0 \end{bmatrix}^T$$

$$\Delta A = \begin{bmatrix} -1/\rho L_s & 0 & 0 & 0 \\ 0 & -1/\rho L_s & 0 & 0 \\ -L'_r/L_m & 0 & 0 & 0 \\ 0 & -L'_r/L_m & 0 & 0 \end{bmatrix} \Delta R_s.$$

By taking Laplace transform of (22) and (23), the transformed equation is given as

$$\Delta y = C(sI - A)^{-1}\left(\Delta A x_0 + B\Delta u\right). \tag{24}$$

Equation of the stator resistance using machine dynamics can be written as

$$\tilde{R}_s = k_p\left[\tilde{i}_{\alpha s}e_{i\alpha s} - \tilde{i}_{\beta s}e_{i\beta s}\right] + k_I\int\left[\tilde{i}_{\alpha s}e_{i\alpha s} - \tilde{i}_{\beta s}e_{i\beta s}\right]dt \tag{25}$$

where $[\,e_{i\alpha s}\ e_{i\beta s}\,]^T = [\,i_{\alpha s} - \tilde{i}_{\alpha s}\ i_{\beta s} - \tilde{i}_{\beta s}]^T$

Fig. 2(c) represents the discrete block diagram of the stator resistance estimator. From Fig. 2(c), the error in continuous domain is described as that $\Delta\varepsilon = H_R(s)\tilde{i}_s\Delta R_s$, where $\tilde{i}_s = [\,\tilde{i}_\alpha\ \tilde{i}_\beta\,]^T$ and $\Delta\varepsilon$ are *dq* axes stator current error.

Considering only the *d*-axis component, the error equation is written as

$$\Delta\varepsilon = H_{R1}(s)\tilde{i}_s\Delta R_s. \tag{26}$$

Therefore, the open loop transfer function of the stator resistance estimator is given in (26) can be written as

$$H_{R1}(s) = \frac{S^3 + S^2p_1 + Sp_2 + p_3}{S^4 + 2S^3p_4 + S^2p_5 + Sp_6 + p_7}. \tag{27}$$

The final closed loop transfer function is given as

$$\frac{\tilde{R}_s}{R_s} = \frac{H_{R1}(s)\tilde{i}_s\left(k_P + k_I\frac{T_s}{2}\frac{z+1}{z-1}\right)}{1 + H_{R1}(s)\tilde{i}\left(k_P + k_I\frac{T_s}{2}\frac{z+1}{z-1}\right)} \tag{28}$$

where

$$p_1 = 2c + a, p_2 = c^2 + 2ac - d^2 - bj,$$
$$p_3 = a(c^2 - d^2) - j(fd + cb),$$
$$p_4 = 2(a + c), p_5 = ((a + c)^2 + 2ac - d^2 - 2bj),$$
$$p_6 = (2(a + c)(ac - bj) - 2i(fj + ad)),$$
$$p_7 = a^2(c^2 - i^2) + j^2(b^2 - e^2) - 2aj(ei + cb)$$
$$a = \frac{L_m^2}{\sigma L_sL_r\tau_r} + \frac{R_s}{\sigma L_s},\ b = \frac{L_m}{\sigma L_sL_r\tau_r},\ c = \frac{1}{\tau_r},\ d = \omega_r,$$
$$j = \frac{L_m}{\tau_r},\ f = \frac{L_m\omega_r}{\sigma L_sL_r}.$$

Discretized form of transfer function given in (28) by replacing $s = \frac{2}{T_s}\frac{z-1}{z+1}$ can be written as follows:

$$H_{R1}(z) = \frac{n_0 + n_1z^{-1} + n_2z^{-2} + n_3z^{-3} + n_4z^{-4}}{d_0 + d_1z^{-1} + d_2z^{-2} + d_3z^{-3} + d_4z^{-4}} \tag{29}$$

where

$$n_0 = 8T_s + 4T_s^2p_1 + 2T_s^3p_2 + T_s^4p_4,$$
$$n_1 = -16T_s + 4T_s^3p_2 + 4T_s^4p_3,$$
$$n_2 = -8T_s^2p_1 + 6T_s^4p_3,$$
$$n_3 = 16T_s - 4T_s^3p_2 + T_s^4p_3,$$
$$n_4 = -8T_s + 4T_s^2p_1 - 2T_s^3p_2 + 4T_s^4p_4,$$
$$d_0 = 16 + 8T_sp_4 + 4T_s^2p_5 + 2T_s^3p_6 + T_s^4p_4,$$
$$d_1 = -64 - 16T_sp_4 + 4T_s^3p_6 + 2T_s^4p_7,$$
$$d_2 = 96 - 8T_s^2p_5 + 6T_s^4p_7,$$
$$d_3 = -64 - 16T_sp_4 - 4T_s^3p_6 + 4T_s^4p_7,$$
$$d_4 = 16 + 8T_sp_4 + 4T_s^2p_5 + 2T_s^3p_6 + T_s^4p_4.$$

B. Rotor Time Constant Adaptation

The rotor time constant τ_r of the IM is estimated. The error matrix $[w]$ for τ_r can be written as, eq (30) and (31) shown at the bottom of this page.

Therefore, the system has forward path matrix with strictly positive real values. Now, to check the stability of nonlinear feedback path matrix, the Popov's inequality criterion is used. By Popov's inequality,

$$\int_0^{t1}\frac{d}{dt}fn(t)fn(t)dt \geq -\frac{fn^2(0)}{2}. \tag{32}$$

The Popov's inequality is satisfied and the solution can be derived as

$$\int_0^{t1}\mathrm{Re}\left(e^Tw\right)dt \geq -\frac{1}{2}\left[\frac{1}{\tilde{\tau}_r} - \frac{1}{\tau_r}\right]^2 \geq -\frac{a_0^2}{2}. \tag{33}$$

$$\Delta A\tilde{x} = w = \begin{bmatrix} \frac{-L_m^2}{\rho L_sL_r'}\left[\frac{1}{\tilde{\tau}_r} - \frac{1}{\tau_r}\right] & 0 & \frac{L_m}{\rho L_sL_r'}\left[\frac{1}{\tilde{\tau}_r} - \frac{1}{\tau_r}\right] & 0 \\ 0 & \frac{-L_m^2}{\rho L_sL_r'}\left[\frac{1}{\tilde{\tau}_r} - \frac{1}{\tau_r}\right] & 0 & \frac{L_m}{\rho L_sL_r'}\left[\frac{1}{\tilde{\tau}_r} - \frac{1}{\tau_r}\right] \\ L_m\left[\frac{1}{\tilde{\tau}_r} - \frac{1}{\tau_r}\right] & 0 & -\left[\frac{1}{\tilde{\tau}_r} - \frac{1}{\tau_r}\right] & 0 \\ 0 & L_m\left[\frac{1}{\tilde{\tau}_r} - \frac{1}{\tau_r}\right] & 0 & \left[\frac{1}{\tilde{\tau}_r} - \frac{1}{\tau_r}\right] \end{bmatrix}\begin{bmatrix} \tilde{i}_\alpha \\ \tilde{i}_\beta \\ \tilde{\varphi}_{\alpha r} \\ \tilde{\varphi}_{\beta r} \end{bmatrix} \tag{30}$$

$$w^Te = e^Tw = \left[\frac{1}{\tilde{\tau}_r} - \frac{1}{\tau_r}\right]\begin{bmatrix} \left(K_M\tilde{i}_\alpha + K_N\tilde{\varphi}_{\alpha r}\right)e_{i\alpha} + \left(K_M\tilde{i}_\beta + K_N\tilde{\varphi}_{\beta r}\right)e_{i\beta} \\ + \left(L_m\tilde{i}_\alpha - \tilde{\varphi}_{\alpha r}\right)e_{\varphi\alpha r} + \left(L_m\tilde{i}_\beta - \tilde{\varphi}_{\beta r}\right)e_{\varphi\beta r} \end{bmatrix} \tag{31}$$

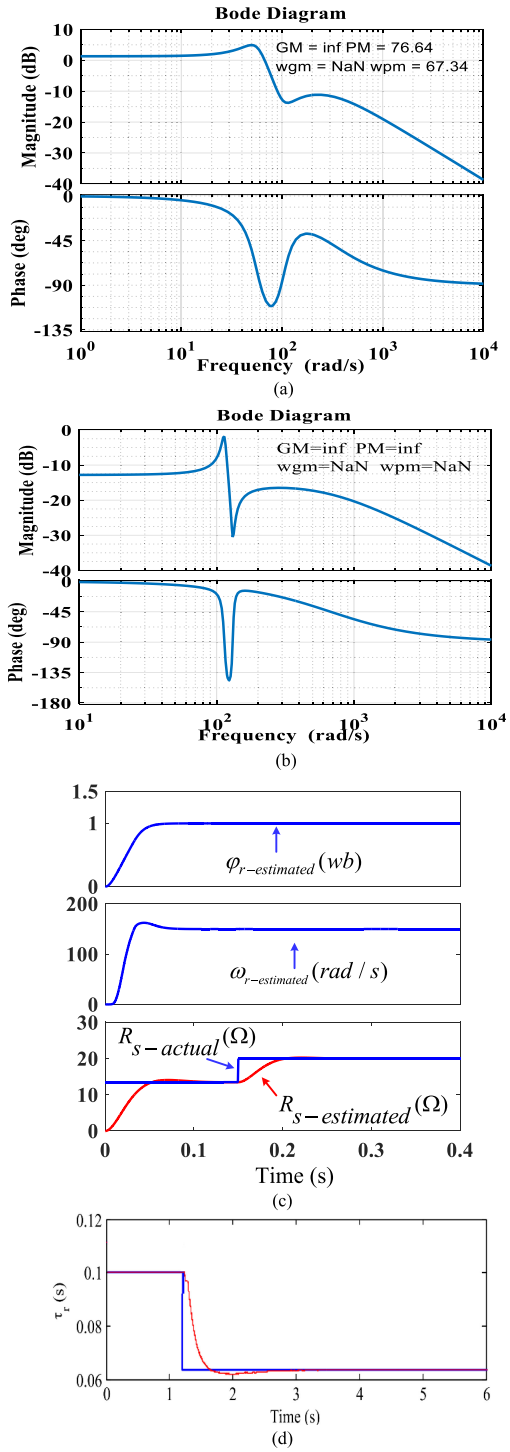

Fig. 3. Stator resistance and rotor time constant adaptation. (a) Bode plot at Rs. (b) Bode plot at 5 Rs. (c) Stator resistance adaption. (d) Rotor time constant adaption.

Therefore, the following inequality satisfies the Popov's theorem. Further, the adaptive rotor-time constant is identified as

$$\frac{1}{\overline{\tau_r}_{ini}} = \int_0^{t1} \frac{d}{dt}\left(\frac{1}{\tilde{\tau}_r}\right) d\tau + \frac{1}{\tilde{\tau}_r}(0)$$
$$= \left(k_p + k_I \frac{T_s}{2}\frac{z+1}{z-1}\right)\left[\tilde{i}_\alpha e_{\psi\alpha r} - \tilde{i}_\beta \varphi_{\beta r}\right] L_m. \quad (34)$$

TABLE I
INDUCTION MOTOR PARAMETERS AND RATINGS

Parameters	Value
Rated power	3 HP
Rated speed(ω_r)	1430 rpm
Number of poles(P)	4
Stator phase voltage(V)	415
Rotor resistance per phase(R_r)	6.82 Ω
Stator resistance per phase (R_S)	13.5 Ω
Rotor leakage inductance per phase(L_{lr})	0.045 H
Stator leakage inductance per phase(L_{lr})	0.045H
Magnetizing inductance per phase (L_m)	0.664H
Rotor inertia(J)	0.00873Kgm^2
Frequency(f)	50 Hz

C. Speed Estimation

The accurate speed estimation involves accurate estimation of motor fluxes in stationary rotor reference frame [23]. Using (9.1), the estimated slip speed is given as

$$\omega_{\mathrm{sl}} = \left(\varphi_{\alpha\,\mathrm{r}} i_{\beta\,\mathrm{s}} - \varphi_{\beta\,\mathrm{r}} i_{\alpha\,\mathrm{s}}\right)/\varphi_r \times \frac{\mathrm{L}_m}{\tau_r} \text{ and}$$
$$\omega_e = \left(\varphi_{\alpha\,\mathrm{s}} \dot{\varphi}_{\beta\,\mathrm{s}} - \varphi_{\beta\,\mathrm{s}} \dot{\varphi}_{\alpha\,\mathrm{s}}\right)/\varphi_s \quad (35)$$

where $\varphi_{\alpha r}$ and $\varphi_{\beta r}$ are rotor fluxes in stationary reference frame, ω_e is the synchronous speed, $\tau_r = L_r/R_r$ is rotor time constant. The motor speed is given as

$$\tilde{\omega}_r = \omega_e - \omega_{\mathrm{sl}}. \quad (36)$$

D. Stability Analysis of the System With Rotor Resistance Adaptation

The stability of the system is analyzed by varying the stator resistance from its nominal value. It is expected that the actual stator resistance is constant. Fig. 3(a) shows the Bode plot of the system at rated stator resistance and the stability is analyzed by observing the gain margin (GM) and the phase margin (PM) of the plot. It is observed that both GM and PM are positive, which implies that the system is stable. Furthermore, the GM is at infinity, which proves the robustness of the parameter estimation method. The adaptability of the system is confirmed for one more operating condition in which the motor resistance is fixed at five times the nominal stator resistance. Fig. 3(b) validates the stability of the system for this large variation in stator resistance under worst operating condition. The GM is infinite in this case, which again validates the robustness of the system.

VII. SIMULATION RESULTS AND DISCUSSIONS

The proposed PCC for DFOC IM drive system is modeled and simulated in MATLAB/Simulink. The results obtained under different operating conditions with conventional PCC and proposed PCC are presented for comparison performance of the drive. The parameters and ratings of IM used for the simulation studies are given in Table I.

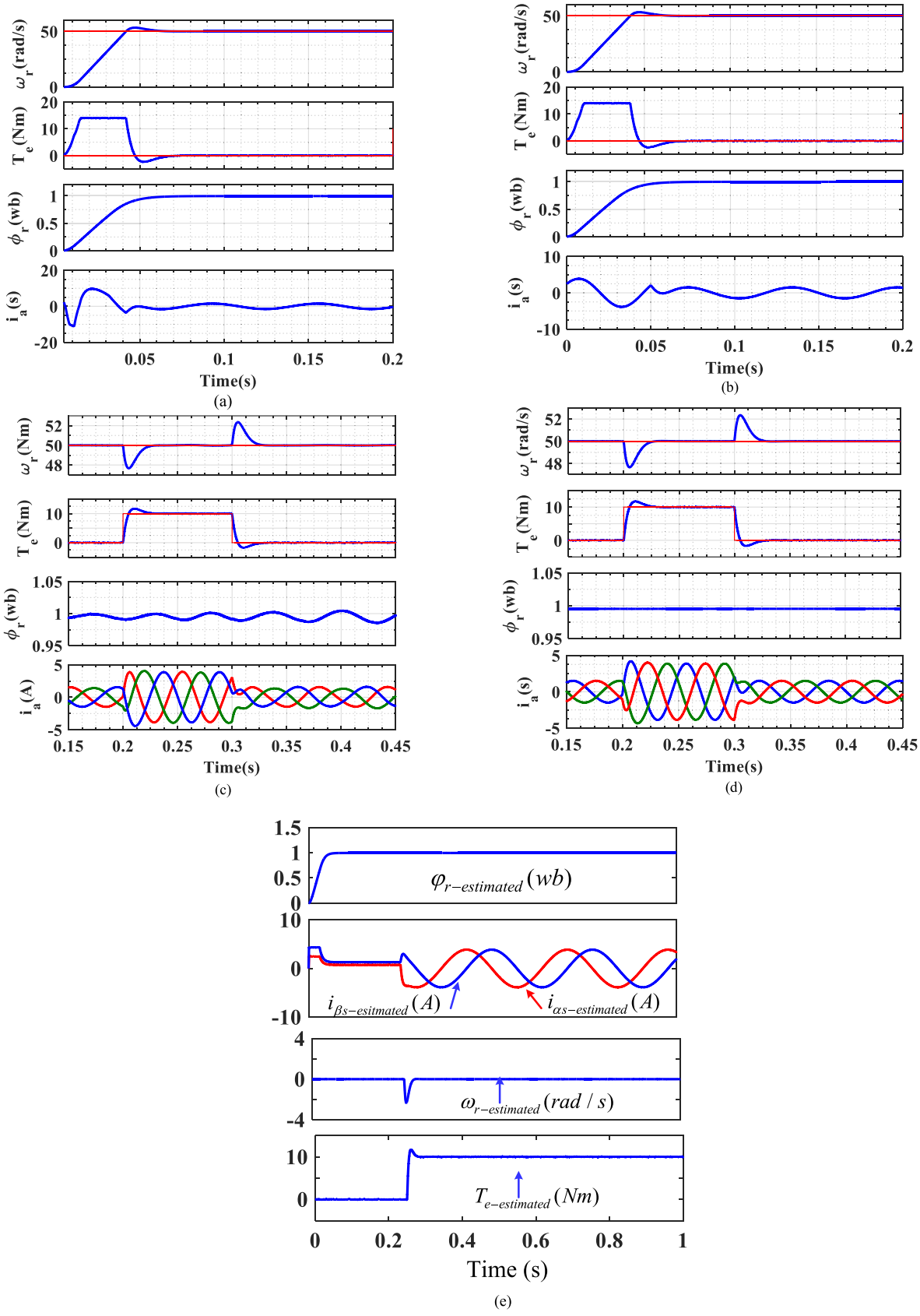

Fig. 4. Starting and load torque dynamic response of IM drive. (a) Starting dynamics with conventional PCC and LPF flux integration. (b) Starting dynamics with proposed PCC and modified LPF flux integration. (c) Load dynamics with conventional PCC and LPF flux integration. (d) Load dynamics with proposed PCC and modified LPF flux integration. (e) Zero speed and load dynamic with proposed PCC and modified LPF flux integration.

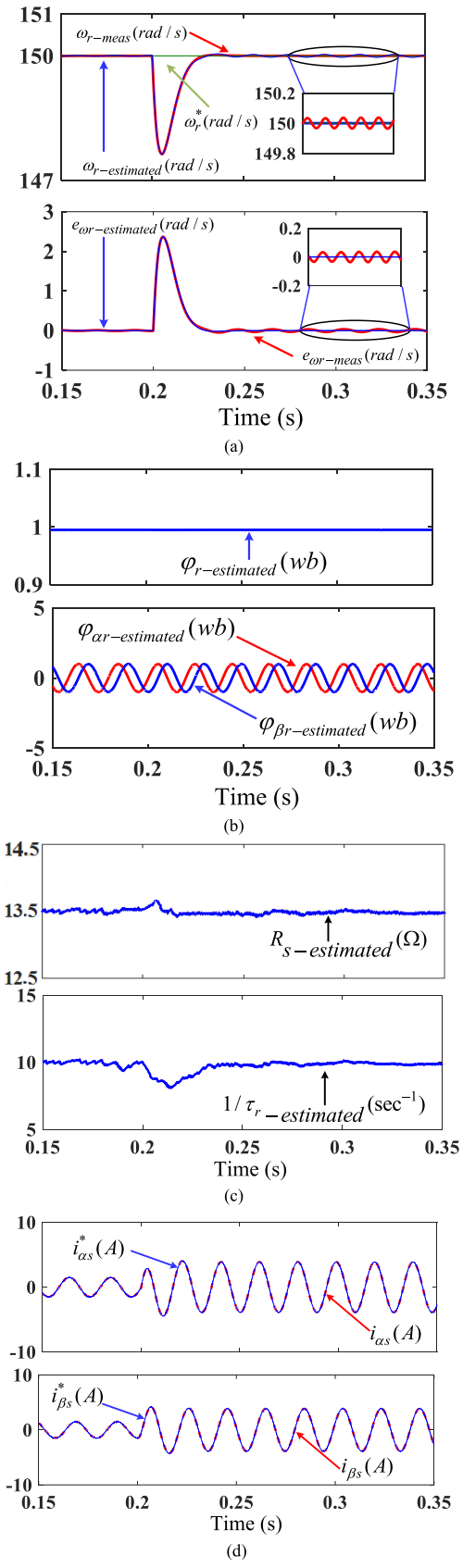

Fig. 5. Load torque dynamic response of IM drive with proposed method. (a) Measured and estimated speed. (b) Measured and estimated flux. (c) Estimated stator resistance and inverse rotor time constant. (d) Reference and measured current components.

A. Motor Stator Resistance and Rotor Time Constant Adaptation

Fig. 3(c) shows the adaptability of the PCC to the stator resistance variation and Fig. 3(d) shows the adaptability of the system to the rotor time constant. Initially, motor runs at 150 rad/s without load and the nominal stator resistance value is 13.5 Ω. It is observed from Fig. 3(c) that estimated value of the stator resistance track the nominal value of stator resistance of the motor. At $t = 0.15$ s, the stator resistance is increased by 50% and it can be observed that the drive performance is satisfactory. Speed and flux in the motor are constant with increased stator resistance value, which proves the robustness of the controller. When rotor time constant reduced by 50% of the rated value it also tracks the reference value as shown in Fig. 3(d). The estimated value of stator resistance and rotor time constant closely track the nominal value of motor parameters with the stable motor operation.

B. Starting Dynamics of IM Drive

The starting behavior of a classical PCC-based DFOC and proposed DFOC IM drive is investigated. The profiles of rotor speed (ω_r), torque (T_e), and rotor flux (φ_r), and stator currents (i_a) are shown for classical PCC-based DFOC and proposed method in Fig. 4(a) and (b), respectively. Initially, the IM runs at low speed 50 rad/s without load. From Fig. 4(a) and (b), it is observed that starting transients in speed, torque, and flux with proposed method is smoother than the classical PCC-based DFOC. It is also observed that the speed and flux response in proposed method is faster than the PCC-based DFOC as it reaches to the steady-state value comparatively in lesser time. The speed of the motor rise to the steady-state value in 0.09 s when conventional PCC-based DFOC is used, whereas it requires 0.08 s with proposed PCC control. The overshoot in speed is 3.3 rad/s in the case of conventional PCC-based FOC, whereas 3.2 rad/s with proposed PCC controlled drive. It is observed that the accuracy of the flux estimation during startup period is improved by the proposed modified flux estimator.

C. Starting Dynamics of IM Drive Under Sudden Load Disturbance and Speed Reversal

Fig. 4(c) and (d) shows the dynamic performance of the IM with the PCC-based DFOC and the proposed PCC method, when a sudden load torque is applied on IM. The IM is driven at $\omega_r = 50$ rad/s and load torque $T_l = 10$ Nm is suddenly applied at $t = 0.2$ s in both cases. When motor runs with the PCC and the proposed PCC-based DFOC, speed is dropped by 2.35 rad/s and then recovers in $t = 0.045$ s to the reference speed as shown in Fig. 4(c) and (d), respectively. The torque developed reaches to the load torque $T_l = 10$ Nm in $t = 0.03$ s as shown in Fig. 4(c) and (d). When load torque is suddenly removed at $t = 0.3$ s, there is an overshoot in speed by 2.36 rad/s but it settles to the reference speed in $t = 0.03$ s by the controller in both the cases. It is also observed in Fig. 4(c) that as soon as motor is loaded, flux has some ripples. However, these ripples are not observed in the proposed PCC controlled drive as shown in Fig. 4(d). There are some ripples in the stator currents of the IM as shown in Fig. 4(c)

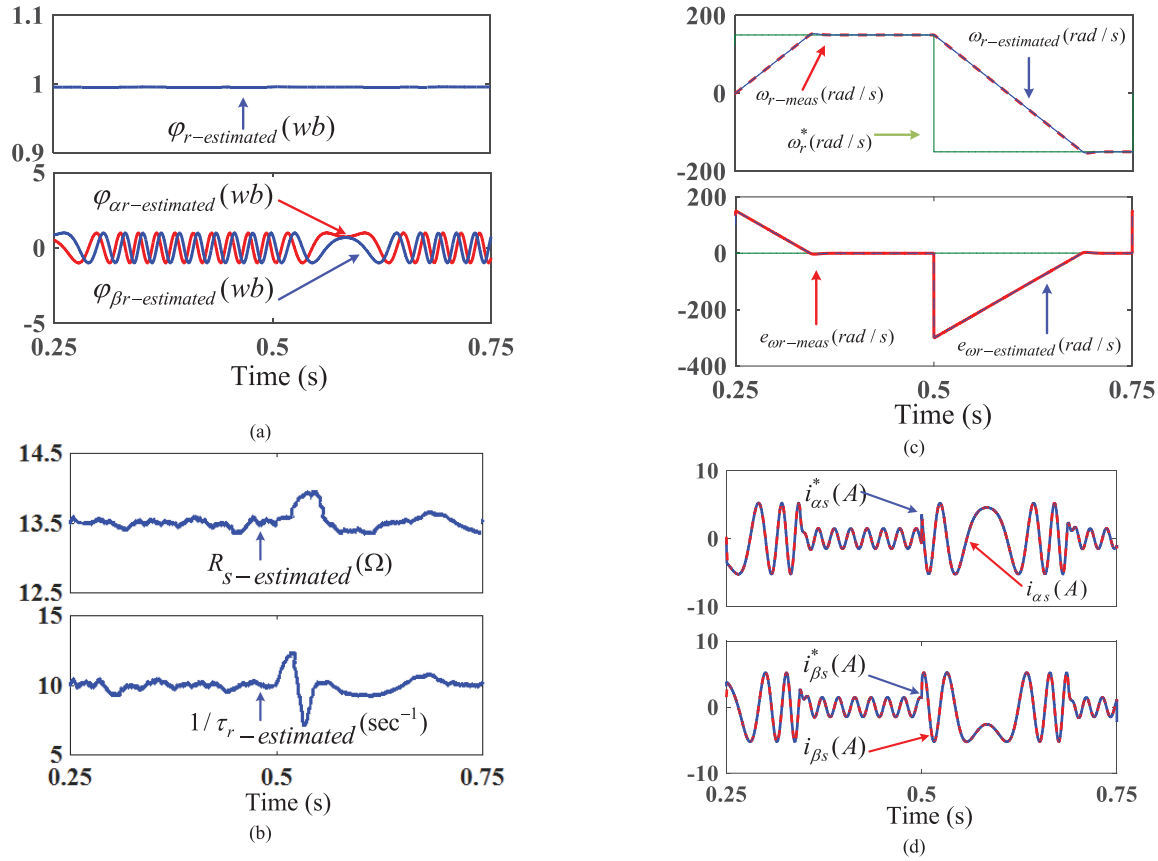

Fig. 6. Speed reversal dynamic response of IM drive with proposed method. (a) Measured and estimated flux. (b) Estimated stator resistance and inverse rotor time constant. (c) Measured and estimated speed. (d) Reference and measured current components.

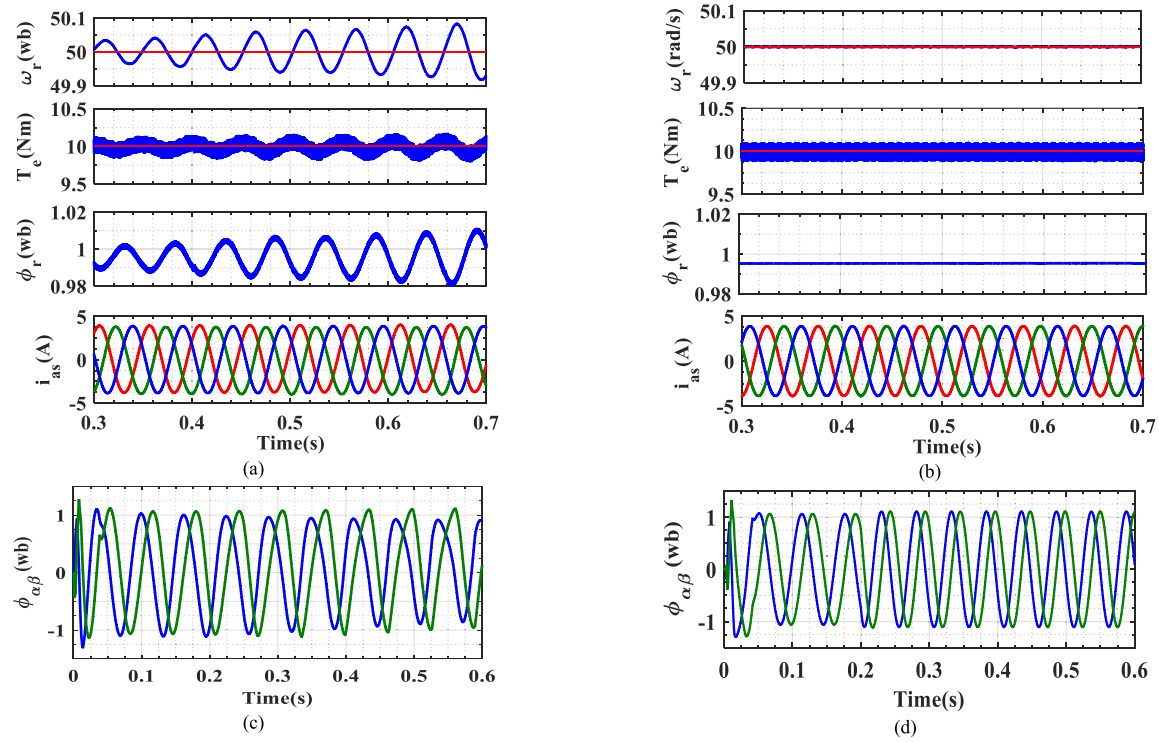

Fig. 7. Steady-state response of IM drive (a), (c) with conventional PCC and LPF flux integration (b), (d) with proposed PCC and modified LPF flux integration.

when motor operates at no load but smoother current response is observed under load conditions as shown in Fig. 4(d). Fig. 4(d) shows that the rotor flux is almost constant even with sudden change in the load torque which also indicates the improved behavior of the IM drive with proposed PCC control. Fig. 4(e) shows the zero speed dynamics of the proposed method. It is observed that motor start smoothly and after 2.5 s, the load torque of 10 Nm is suddenly applied. It can be observed from Fig. 4(e) that speed drops momentarily but it recovers quickly to reference level and reaches its steady-state value in few seconds. The flux is observed to be constant even after the change in load. The current $i_{\alpha s}$ and $i_{\beta s}$ are constant initially as there is no frequency at zero speed. The overall, dynamic performance of the motor is stable and satisfactory at zero speed.

Effect of the load torque on measured speed, estimated speed, speed error, flux, stator resistance, inverse rotor time constant, reference, and estimated components of stator currents are shown in Fig. 5(a)–(d), respectively with the proposed controller. Effect of sudden change in load torque is observed as small deviation in estimated stator resistance and inverse rotor time constant but this deviation is recovered by the controller in next few seconds and the estimated values of all these parameters and variables are settled at their steady-state values quickly. The speed reversal performance of the motor is specially demonstrated through measured speed, estimated speed, speed error, flux, stator resistance, inverse rotor time constant, reference, and estimated components of current in Fig. 6(a)–(d), respectively with the proposed controller. The speed reversal of the speed from 150 to -150 rad/s is made by varying reference speed. It is observed that estimated inverse rotor time constant and stator resistance have very small deviation in magnitude. However, the estimated quantities recover to its nominal value and reach its steady-state values quickly.

D. Steady-State Response of IM Drive

Fig. 7(a) and (b) shows zoomed waveform of the steady-state behavior of the motor rotor speed (ω_r), torque (T_e), rotor flux (φ_r), and stator current i_a. Fig. 7(c) and (d) shows the steady-state behavior of $\varphi_{\alpha\beta}$ when PCC-based DFOC with LPF flux estimator and proposed DFOC with modified flux estimator is used, respectively. It is clearly observed in Fig. 7(a) that the speed, torque, and rotor flux have some ripples. However, there are no such ripples observed in Fig. 7(b) and (c). Fig. 5(d) shows the $\alpha\beta$-stator flux waveforms when a small dc signal is introduced to the back-emf signal. It is observed that there is dc drift in the estimated flux and small flux distortions in classical method. However, dc drift problem and distortion in flux is resolved using the proposed flux eliminated method. Sampling period for simulation in both the cases is $T_s = 2\,\mu$s.

VIII. Experimental Results and Discussions

Fig. 8 shows the photograph of the experimental prototype setup used for experimental validation of the proposed PCC control of DFOC IM drive. A complete schematic diagram is shown in Fig. 1(a) and (b). The DFOC IM drive consists

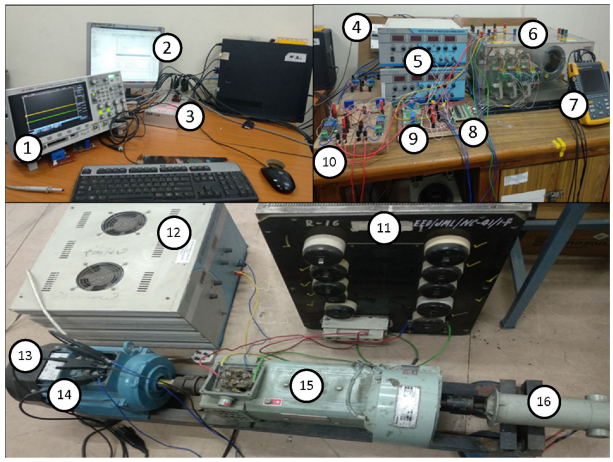

Fig. 8. Experimental prototype setup: 1—four channel digital oscilloscope, 2—PC, 3—dSPACE 1104, 4—grid, 5—dc power supply, 6—three phase rectifier plus inverter, 7—three phase power analyzer, 8—driver circuit, 9—current sensor, 10—voltage sensor, 11—resistive load, 12—300 V dc power supply, 13—three phase induction motor, 14—voltage probe, 15—dc generator, 16—tachogenerator.

of the VSI, driver circuit, dS dsp1104 controller, current sensors, and power supplies. The dSPACE system with dS1104 TMS320F240 controller board with MATLAB/Simulink is used for implementing control strategy. The different controllers are implemented and operation of drive is analyzed under different operating conditions for real-time validation. The parameters of drive used for the experimental study is given in Table I. The stator voltage to the IM is fed by the VSI, which is controlled by the gate pulses produced through dS1104 controller using different control algorithms. A dc machine is coupled with IM to arrange electrical loading on the IM. Stator currents of the IM are sensed by the two current sensors. A four channel digital storage oscilloscope is used for the recording the waveform of IM under different operating conditions. The sampling time of the control structure is selected at 50 μs in both the cases.

A. Performance of the IM Drive During Starting

Fig. 9 shows the starting response of the IM drive with classical and proposed method. Fig. 9(a) and (b) shows the starting response of the rotor speed (ω_r), torque (T_e), stator current ($i_{\alpha s}$), and stator currents ($i_{\beta s}$). The IM requires few seconds to reach to the steady-state speed and the torque developed is adequate enough to rotate the rotor on steady-state level. It is observed that the current drawn by the motor during starting is high in magnitude but it reduces to no load current level. The dynamic response of the drive using proposed method is observed to be faster than the classical PCC-based DFOC. Fig. 9(c) and (d) shows the response of the α-axis flux ($\varphi_{\alpha s}$), β-axis flux ($\varphi_{\beta s}$), α-axis stator current ($i_{\alpha s}$), and β-axis stator currents ($i_{\beta s}$). These waveforms are observed to have lesser ripple in the case of proposed method than the classical PCC-based DFOC.

B. Performance of the IM Drive on Load

Fig. 10(a) and (b) shows the dynamic response of the motor rotor speed (ω_r), torque (T_e), and stator current (i_{as}) with

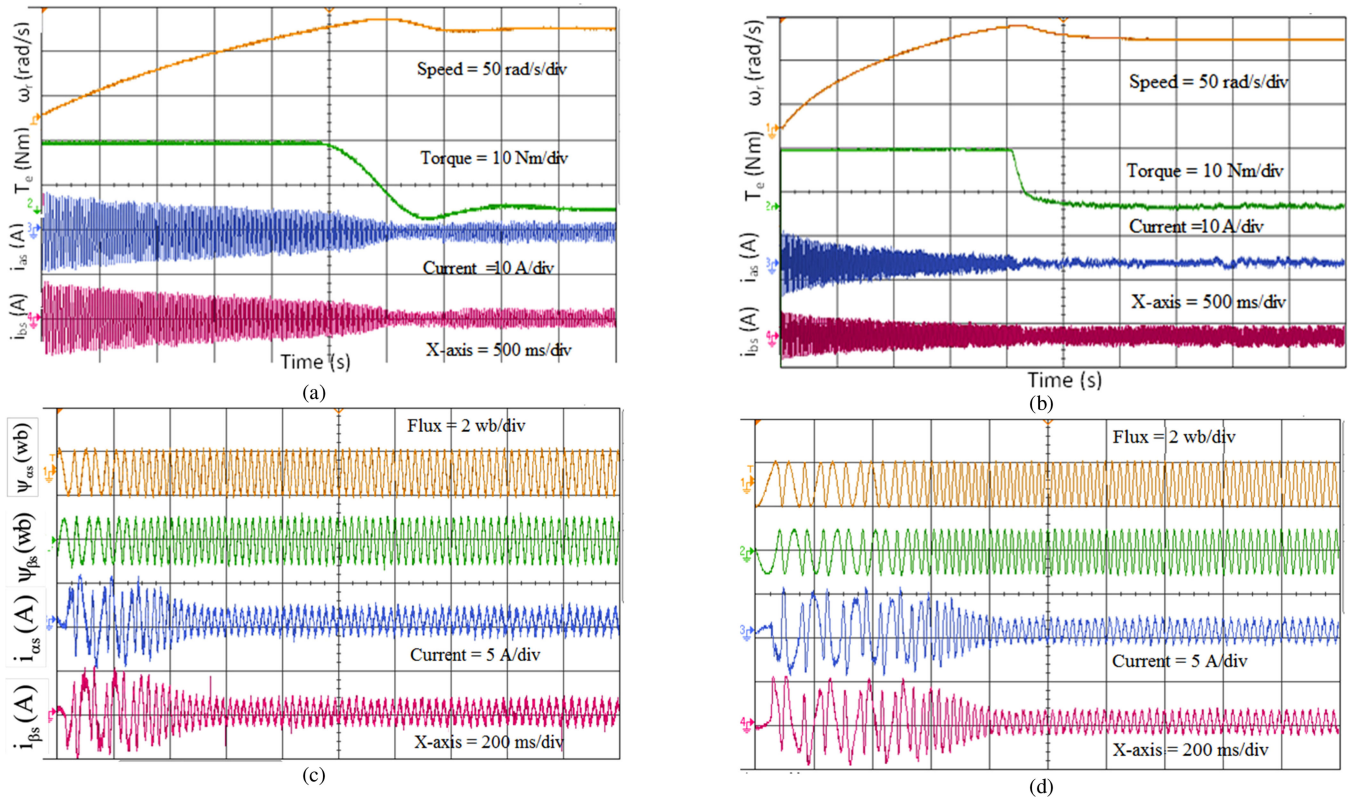

Fig. 9. Starting response of IM drive (a), (c) with conventional PCC and LPF flux integration (b), (d) with proposed PCC and modified LPF flux integration.

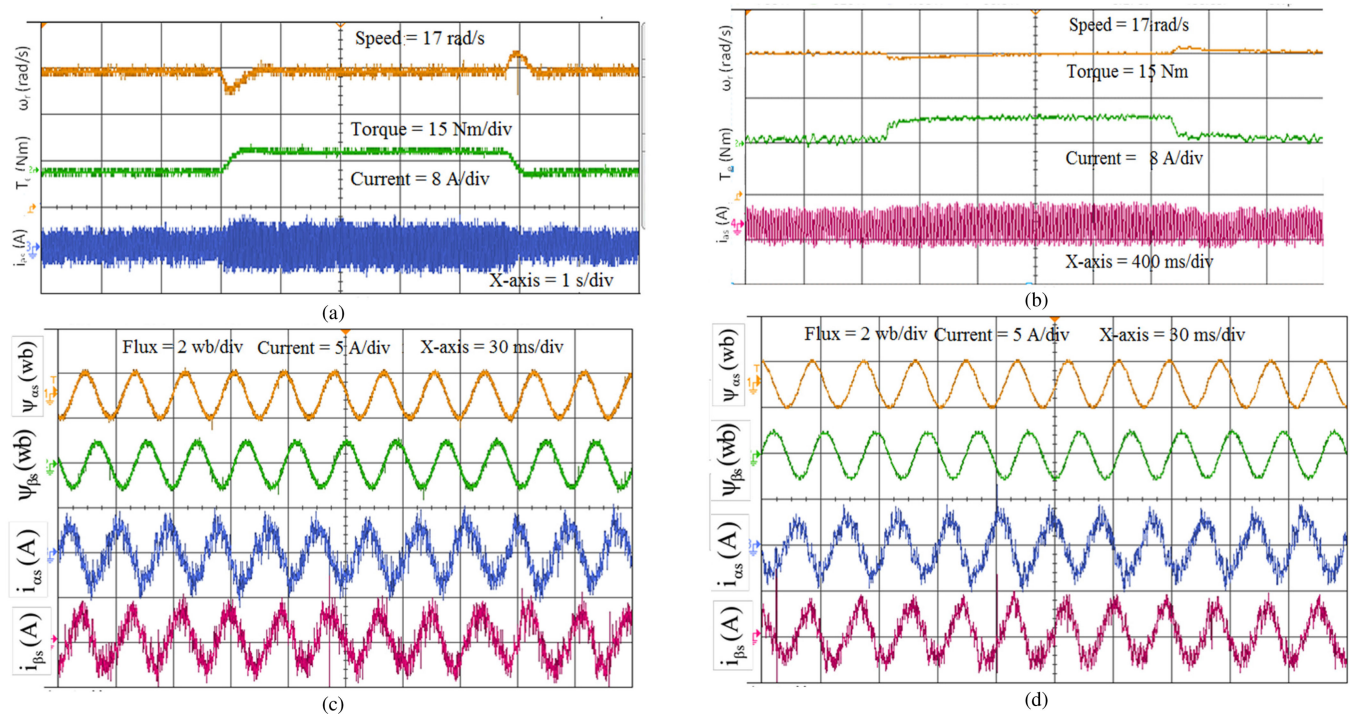

Fig. 10. Load response of IM drive (a), (c) with conventional PCC and LPF flux integration (b), (d) with proposed PCC and modified LPF flux integration.

conventional PCC and proposed PCC, respectively. Fig. 10(c) and (d) shows the response of the α-axis flux ($\varphi_{\alpha s}$), β-axis flux ($\varphi_{\beta s}$), α-axis stator current ($i_{\alpha s}$), and β-axis stator currents ($i_{\beta s}$) for classical PCC-based DFOC and proposed drive, respectively. In Fig. 10(a) and (b), the load torque is suddenly changed to 10 Nm and it is observed that motor current increases to increase the motor torque and motor speed settles to reference speed in few seconds. After few seconds, the load torque is suddenly removed and speed of the motor overshoot for short interval but it settled down to reference speed. Torque and speed response is observed to be faster in the case of proposed method.

Fig. 10(c) and (d) also show the steady-state response of the stator fluxes in the case of classical PCC-based DFOC and proposed method. Steady-state response of proposed method is observed to be better than the classical method.

C. Performance of the IM Drive Under Sudden Change in Speed

Fig. 11(a) and (b) show the speed reversal dynamics from 50 to -50 rad/s and 30 to -30 rad/s with PCC-based DFOC and proposed method. Zoomed speed response of speed reversal from 50 to -50 rad/s is also shown to demonstrate the effect of controller at zero crossing. It is closely observed that the speed reversal dynamics of the motor is faster with proposed method. Phase sequence reversal of the current is also observed. At zero crossing, speed and torque are also found to have smooth response with proposed method compared to that in the classical method.

Fig. 11(c) shows the reference speed, estimated speed with PCC-based DOFC, estimated speed with proposed method and speed error between reference speed and estimated speed with PCC-based DFOC. Starting speed transients are observed smoother in the case of proposed method.

Fig. 12(a) shows the effect of variations in speed on stator resistance in proposed techniques. It is observed that initially when motor runs at speed 50 rad/s, estimated stator resistance is 13.5 Ω. After few seconds, speed changes from 50 to -50 rad/s, it is observed that there is small glitch in estimated value of stator resistance but settles down to its rated value. In next few seconds, speed reduces from -50 rad/s to zero and it is observed that the estimated stator resistance remains at its rated value except a small dip during transient period. It shows the robustness of the proposed controller. Fig. 12(b) shows the steady-state response of the rotor flux with the proposed method.

Fig. 12(c) shows the effect of stator resistance variations. Initially, motor is set to run at 50 rad/s at 50% of the full load with rated stator resistance. When estimated speed, flux, and stator resistance of motor attain steady-state value, the stator resistance is increased by inserting external resistance into stator winding in series. The estimated speed and flux settle to their reference value with small disturbances during transient state. The estimated stator resistance is observed to track the change in actual value closely.

Fig. 12(d) shows the effect of the step change in speed on inverse rotor time constant. Initially, motor is set to run at 50 rad/s so that the estimated speed, measured speed, and inverse rotor time constant attain steady-state value. After some time, the speed changes from 50 to 100 rad/s and it is observed that estimated and measured speed, closely follow the reference speed. There is a small change in rotor time constant during the transient state but it settles down to its rated value in next few seconds, which shows the robustness of inverse rotor time constant against speed variations.

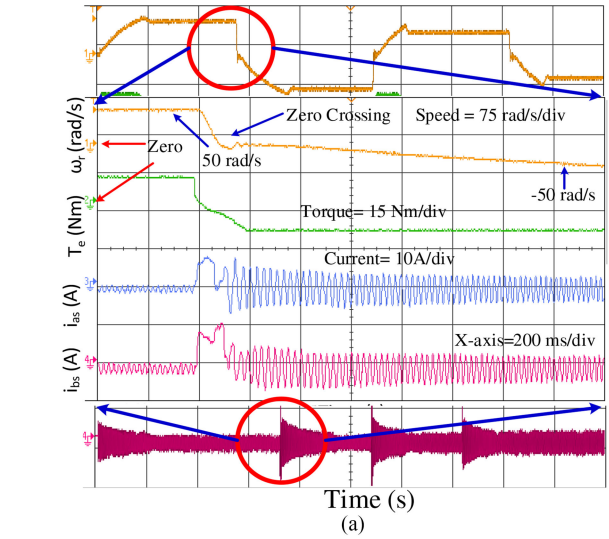

(a)

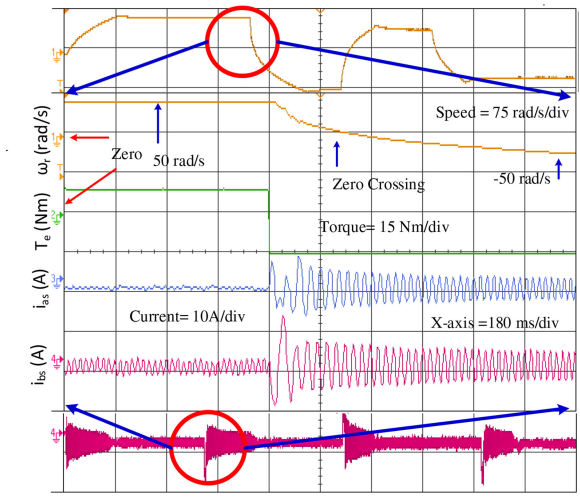

(b)

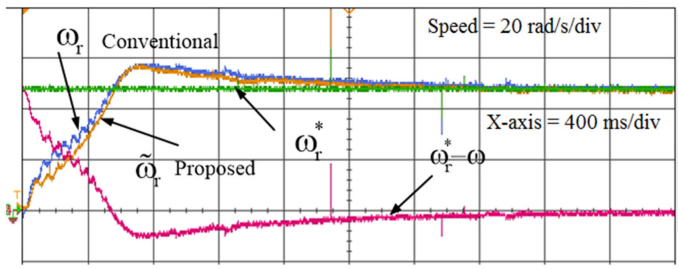

(c)

Fig. 11. Speed reversal dynamics of IM drive. (a) With conventional PCC and LPF flux integration. (b) With proposed PCC and modified LPF flux integration. (c) Speed response with conventional PCC and LPF flux integration and proposed PCC and modified LPF flux integration.

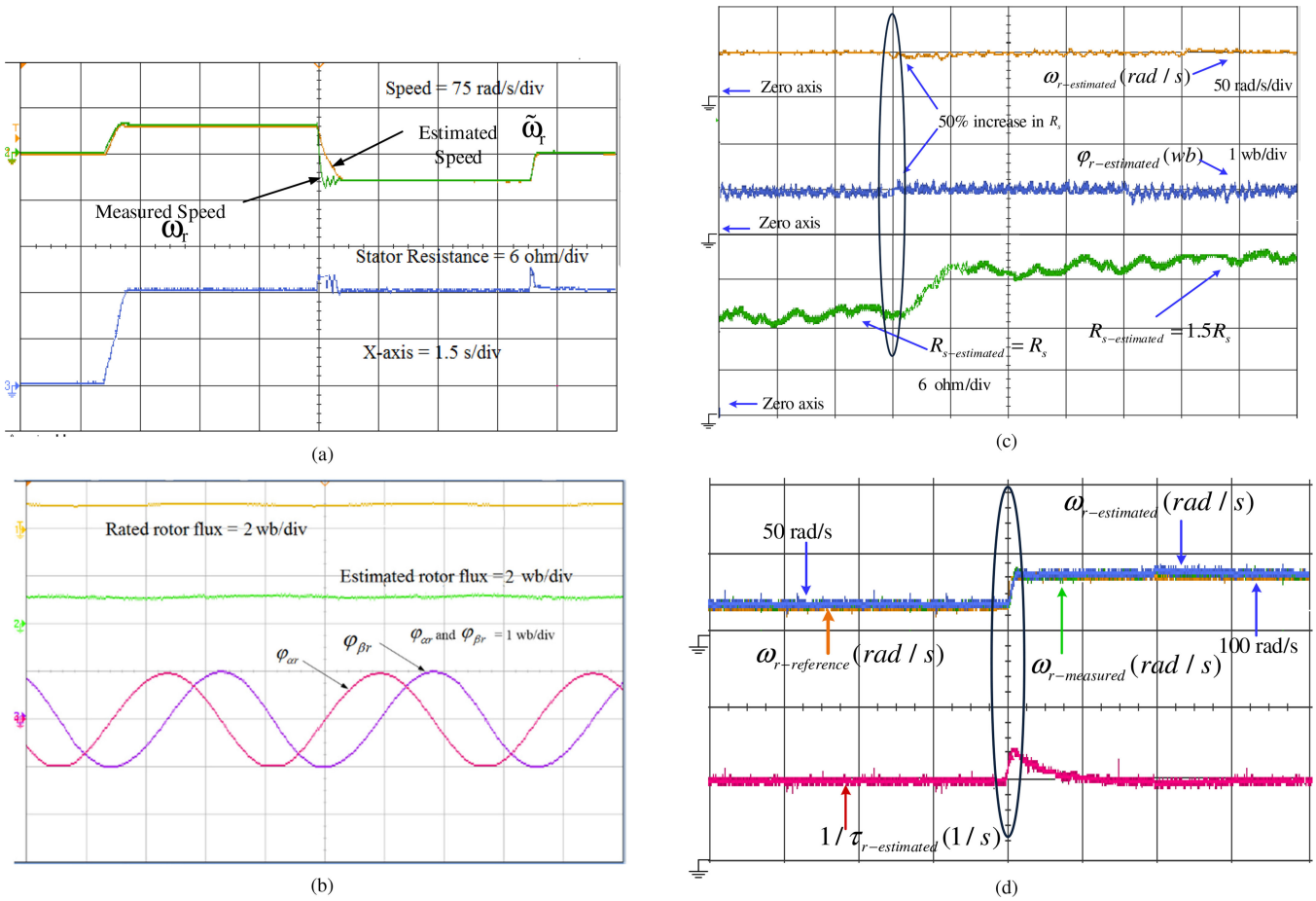

Fig. 12. (a) Speed reversal and its effect on estimated stator resistance. (b) Rotor flux in steady state. (c) Change in stator resistance and its effect on speed and flux. (d) Change of reference speed and its effect on inverse rotor time constant.

Simulation and experimental investigations validate the effectiveness of the proposed adaptive PCC-based DFOC of IM drive under dynamic and steady-state study conditions.

IX. Conclusion

The performance analysis of PCC-based sensorless DFOC IM drive with pure integrator voltage model flux estimator and adaptive PCC-based DFOC IM drive with modified LPF voltage model flux estimator are investigated through simulation and experimentation. The stator resistance of the motor is estimated for implementation of adaptive PCC in DFOC of IM drive. Robustness and stability of the system with variation in the stator resistance is validated in frequency domain using Bode plot. Robustness of the drive against rotor time constant is verified using Popov's stability criteria. The proposed method is capable to overcome, parameter mismatches, current and voltage detection errors, unknown integral initial value problem and problems caused by dc offset, effectively. The usefulness of proposed method is demonstrated in low-speed region of operation for DFOC IM drive and it also gives better dynamic response especially better speed reversal, starting, and low steady-state speed error. The experimental and simulation results show that the proposed PCC can effectively improve the dynamic and steady-state performance of IM drive.

References

[1] L. Malesani and P. Tomasin, "PWM current control techniques of voltage source converters—A survey," in *Proc. 19th Annu. Conf. IEEE Ind. Electron.*, 1993, pp. 670–675.

[2] L. Zhang and H. R. Tayebi, "Field-oriented CSI induction motor drive with optimal predictive current regulation," in *Proc. 5th Int. Conf. Power Electron. Variable-Speed Drives*, London, U.K., 1994, pp. 48–53.

[3] L. Zhang, R. Norman, and W. Shepherd, "Long-range predictive control of current regulated PWM for induction motor drives using the synchronous reference frame," *IEEE Trans. Control Syst. Technol.*, vol. 5, no. 1, pp. 119–126, Jan. 1997.

[4] H. Abu-Rub, J. Guzinski, Z. Krzeminski, and H. A. Toliyat, "Predictive current control of voltage source inverters," in *Proc. 27th Annu. Conf. IEEE Ind. Electron. Soc. (Cat no. 37243)*, vol. 2, 2001, pp. 1195–1200.

[5] H. Abu-Rub, J. Guziński, Z. Krzeminski, and H. A. Toliyat, "Predictive current control of voltage-source inverters," *IEEE Trans. Ind. Electron.*, vol. 51, no. 3, pp. 585–593, Jun. 2004.

[6] R. Kennel, E. El-Kholy, S. Mahmoud, A. El-Refaei, and F. Elkady, "A simple high performance current control scheme for induction motor drives," in *Proc. IEEE 31st Annu. Conf. Ind. Electron. Soc.*, 2005, Paper 6.

[7] J. Rodriguez *et al.*, "Predictive current control of a voltage source inverter," *IEEE Trans. Ind. Electron.*, vol. 54, no. 1, pp. 495–503, Feb. 2007.

[8] P. Cortes *et al.*, "Predictive control in power electronics and drives," *IEEE Trans. Ind. Electron.*, vol. 55, no. 12, pp. 4312–4324, Dec. 2008.

[9] N. Kutasi, A. Kelemen, and M. Imecs, "Vector control of induction motor drives with model based predictive current controller," in *Proc. IEEE Int. Conf. Comput. Cybern.*, 2008, pp. 21–26.
[10] J. M. Retif, L.-S. Xuefang, and F. Morel, "Predictive current control for an induction motor," in *Proc. IEEE Power Electron. Specialists Conf.*, 2008, pp. 3463–3468.
[11] T. Laczynski and A. Mertens, "Predictive stator current control for medium voltage drives with LC filters," *IEEE Trans. Power Electron.*, vol. 24, no. 11, pp. 2427–2435, Nov. 2009.
[12] C. S. Lim, N. A. Rahim, W. P. Hew, M. Jones, and E. Levi, "Model predictive current control of a five-phase induction motor," in *Proc. 37th Annu. Conf. IEEE Ind. Electron. Soc.*, 2011, pp. 1934–1940.
[13] J. Prieto, F. Barrero, C. S. Lim, and E. Levi, "Predictive current control with modulation in asymmetrical six-phase motor drives," in *Proc. 15th Int. Power Electron. Motion Control Conf.*, 2012, pp. 1–8.
[14] J. Guzinski and H. Abu-Rub, "Speed sensorless induction motor drive with predictive current controller," *IEEE Trans. Ind. Electron.*, vol. 60, no. 2, pp. 699–709, Feb. 2013.
[15] S. Wei, Y. Yong, X. Dianguo, X. Jin, and D. Li, "Predictive current control method in induction motor speed sensorless drive," in *Proc. Int. Power Electron. Conf.*, 2014, pp. 341–345.
[16] H. Guzman, F. Barrero, S. Member, M. J. Duran, and I. O. P. M. Ode, "IGBT-gating failure effect on a fault-tolerant induction motor drive," *IEEE Trans. Ind. Electron.*, vol. 62, no. 1, pp. 15–20, Jan. 2015.
[17] Z. Hu and K. Hameyer, "Robust predictive current control for performance improvement of induction motors with parameter variation," in *Proc. 41st Annu. Conf. IEEE Ind. Electron. Soc.*, 2015, pp. 000451–000456.
[18] B. Wang, H. Wang, Y. Yu, X. Lv, G. Wang, and Di. Xu, "Sensorless robust predictive current control for induction motor using a speed adaptive full-order observer," in *Proc. 9th Int. Conf. Power Electron.*, 2015, pp. 1149–1154.
[19] M. Ciobotaru, R. Teodorescu, and F. Blaabjerg, "A new single-phase PLL structure based on second order generalized integrator," in *Proc. 37th IEEE Power Electron. Specialists Conf.*, Jeju, South Korea, 2006, pp. 1–6.
[20] M. Hinkkanen and J. Luomi, "Modified integrator for voltage model flux estimation of induction motors," *IEEE Trans. Ind. Electron*, vol. 50, no. 4, pp. 818–820, Aug. 2003.
[21] Z. Xin, R. Zhao, F. Blaabjerg, L. Zhang, and P. C. Loh, "An improved flux observer for field-oriented control of induction motors based on dual second-order generalized integrator frequency-locked loop," *IEEE J. Emerg. Sel. Topics Power Electron.*, vol. 5, no. 1, pp. 513–525, Mar. 2017.
[22] W. Xu, Y. Jiang, C. Mu, and F. Blaabjerg, "Improved nonlinear flux observer based second-order SOIFO for PMSM sensorless control," *IEEE Trans. Power Electron.*, vol. 34, no. 1, pp. 565–579, Jan. 2019.
[23] J. Guzinski and H. Abu-Rub, "Speed sensorless induction motor drive with predictive current controller," *IEEE Trans. Ind. Electron.*, vol. 60, no. 2, pp. 699–709, Feb. 2013.
[24] A. Devanshu, M. Sinah, and N. Kumar, "Predictive current control of feedback linearized induction motor drive," in *Proc. 3rd IEEE Int. Conf. Intell. Transp. Eng.*, Singapore, 2018, pp. 132–136.
[25] J. Wang, F. Wang, G. Wang, S. Li, and L. Yu, "Generalized proportional integral observer based robust finite control set predictive current control for induction motor systems with time-varying disturbances," *IEEE Trans. Ind. Inform.*, vol. 14, no. 9, pp. 4159–4168, Sep. 2018.

Ambrish Devanshu was born in Patna, India, in 1989. He received the B.Tech. degree in electrical and electronics engineering from the School of Engineering, Cochin University of Science and Technology, Cochin, Kerala, India in 2011.

From September 2011 to June 2014, he was a Project Engineer with Wipro Technologies, Greater Noida, India. Thereafter, he has joined the Department of Electrical Engineering, Delhi Technological University, New Delhi, India, as a Full-Time Ph.D. Research Scholar. His research interests include electric machine drives and power electronics.

Madhusudan Singh was born in Ghazipur, India, in 1968. He received the B.Sc. degree in electrical engineering from the Faculty of Technology, Dayalbagh Educational Institute, Dayalbagh Agra, India, in 1990, the M.E. degree from the University of Allahabad, Allahabad, India, in 1992, and the Ph.D. degree from the Faculty of Technology, University of Delhi, New Delhi, India, in 2006.

In 1992, he joined the Department of Electrical Engineering, North Eastern Institute of Science and Technology, Nirjuli, India, as a Lecturer. In June 1996, he joined the Department of Electrical Engineering, Institute of Engineering and Technology Lucknow, Lucknow, India, as a Lecturer. In March 1999, he joined the Department of Electrical Engineering, Delhi College of Engineering (now Delhi Technological University), New Delhi, India, as an Assistant Professor, where he became a Professor of electrical engineering in 2007. His research interests include modeling and analysis of electrical machines, voltage control aspects of self-excited induction generators, power electronics, and drives.

Narendra Kumar received the B.E. degree from Indian Institute of Technology Roorkee, Roorkee, India, in 1985, the M.E. from Punjab Engineering College, Chandigarh, India, in 1987, and the Ph.D. degree in electrical engineering from Delhi College of Engineering (now Delhi Technological University), New Delhi, India, in 2003.

He is currently a Professor with the Department of Electrical Engineering, Delhi Technological University. His current research interest is power electronics applications in power systems, instrumentation, and control.